



# Structural, electrical, and optical properties of Sb-doped SnO<sub>2</sub> transparent conductive oxides fabricated using an electrospray technique

Bon-Ryul Koo, Hyo-Jin Ahn\*

Department of Materials Science & Engineering, Seoul National University of Science and Technology, Seoul 139-743, Republic of Korea

Received 30 July 2013; received in revised form 17 August 2013; accepted 26 August 2013

Available online 12 September 2013

## Abstract

Sb-doped SnO<sub>2</sub> (ATO) thin films, for use as transparent conductive oxides (TCOs), were synthesized using an electrospray technique, and their structural, electrical, and optical properties were investigated. To elucidate the optimum fabrication conditions for the best electrical and optical properties, ATO thin films were calcined using four different temperatures, 450 °C, 550 °C, 650 °C, and 750 °C. When calcined at 650 °C, ATO thin films exhibit excellent resistivity ( $\sim 8.14 \times 10^{-3} \Omega \text{ cm}$ ), superior transmittance ( $\sim 91.4\%$  at 550 nm), and good figure of merit ( $\sim 11.4 \times 10^{-4} \Omega^{-1}$ ) compared to the other samples. The enhanced properties of ATO thin films are attributed to high densification without formation of cracks, and the increased grain size of ATO nanoparticles.

© 2013 Elsevier Ltd and Techna Group S.r.l. All rights reserved.

**Keywords:** A. Films; A. Calcination; C. Electrical properties; C. Optical properties; Electrospray

## 1. Introduction

Films fabricated using transparent conductive oxides (TCOs) that have a high visible light transparency ( $> 80\%$ ) and low resistivity ( $< 10^{-4} \Omega \text{ cm}$ ) have attracted significant interest recently for use in optoelectronic applications such as solar cells, infrared reflectors, flat panel displays, touch screens, and electrochromic devices [1–4]. To date, several researchers have studied TCO materials such as In<sub>2</sub>O<sub>3</sub>:Sn (ITO), SnO<sub>2</sub>:Sb (ATO), SnO<sub>2</sub>:F (FTO), ZnO:Al (AZO), and ZnO:Ga (GZO). Among the various TCO materials, ATO films are currently of considerable interest due to their excellent thermal and chemical stabilities, good mechanical durability, abundance, and low cost compared to the more widely used ITO materials. Hence, ATO thin films have attracted attention as promising materials for replacing ITO because of their high transparency ( $\sim 80\%$ ) and low resistivity ( $\sim 10^{-3} \Omega \text{ cm}$ ) [5]. In order to fabricate high-quality ATO films, various synthetic methods such as sol–gel spin coating, spray pyrolysis, chemical vapor deposition, vacuum

evaporation, and sputtering have been developed [5–9]. Among the above-mentioned synthetic methods, solution-based TCO thin films, such as spray pyrolysis and sol–gel spin coating, are of great interest due to advantages such as relatively low production cost and a simple manufacturing process. So far, several studies have been devoted to developing high-performance solution-based TCOs. For example, Burgard et al. reported that Sb-doped SnO<sub>2</sub> thin films were synthesized using a spin coating process and their electrical resistivity and transmittance at optimum Sn content was  $2.5 \times 10^{-2} \Omega \text{ cm}$  and 90%, respectively [10]. Bisht et al. synthesized Sb-doped SnO<sub>2</sub> thin film using a spray pyrolysis technique and reported the electrical ( $1.0 \times 10^{-3} \Omega \text{ cm}$ ) and optical (75%) properties [11]. Dua et al. demonstrated Mn–Sb co-doped SnO<sub>2</sub> thin films with a resistivity of  $1.42 \times 10^{-2} \Omega \text{ cm}$  and transmittance of  $\sim 81\%$  using a dip coating technique, referring to the possibility of using co-doped SnO<sub>2</sub> materials as TCOs [12]. Therefore, it is important to develop a novel synthetic method for fabricating high-performance solution-based ATO thin films.

In this paper, the synthesis of solution-based ATO thin films using an electrospray technique is reported for the first time. Further, the structural, chemical, electrical, and optical

\*Corresponding author. Tel.: +82 2 970 6622; fax: +82 2 973 6657.

E-mail address: [hjahn@seoultech.ac.kr](mailto:hjahn@seoultech.ac.kr) (H.-J. Ahn).

properties of these thin films at four different calcination temperatures were examined. An electro spray technique is chosen in particular because of advantages such as a simplicity, cost effectiveness, facile operation, and continuous production of nano-size particles.

## 2. Experimental

### 2.1. Experimental

Four different types of the ATO thin films were prepared using the electro spray technique at temperatures of 450 °C, 550 °C, 650 °C, and 750 °C. To fabricate the solution-based ATO thin films, we set up an electro spray apparatus consisting of a power supply, a syringe with a pump, and a collector, as shown in Fig. 1. Tin(II) chloride dehydrate ( $\text{SnCl}_2 \cdot 2\text{H}_2\text{O}$ , Aldrich) and antimony(III) chloride ( $\text{SbCl}_3$ , Aldrich) were dissolved in 2-propanol (2 mL) for 1 h, and the molar ratio of Sn:Sb was adjusted to 10:1. Furthermore, many researchers reported on the optimum composition of the Sb doping in the  $\text{SnO}_2$  lattice. That is, the optimum molar ratio of Sn:Sb=10:1 shows good agreement with the previously reported results [13,14]. In this manuscript, this composition is chosen because the best performance of the TCO thin films presents. The prepared mixture is used as the solution for the electro spray process. The ATO solution is then loaded into a plastic syringe equipped with a 23-gauge stainless steel needle. The distance between the tip of the needle and the collector is maintained at ~10 cm. The feed rate is controlled at 0.03 mL/h and the voltage applied is 24 kV. ATO nanoparticles were directly deposited on a glass substrate (Corning EAGLE XG™ glass) using the electro spray process. The as-prepared ATO thin films are dried at 150 °C in a convection oven and are annealed at

four different temperatures—450 °C, 550 °C, 650 °C, and 750 °C (corresponding samples are referred to as samples A, B, C, and D)—to determine the optimum conditions for the desired structural, chemical, electrical, and optical properties.

### 2.2. Characterization

The crystalline structure and chemical bonding states of the samples were characterized using X-ray diffraction (XRD, Rigaku D/Max-2500 diffractometer using  $\text{Cu K}\alpha$  radiation) and X-ray photoelectron spectroscopy (XPS, ESCALAB 250 equipped with an  $\text{Al K}\alpha$  X-ray source). The surface morphology of the thin films was analyzed using means of field-emission scanning electron microscopy (FE-SEM, Hitachi S-4700). Structural analyses of the ATO nanoparticles were performed by transmission electron microscopy (TEM, JEOL-2100F operated at 200 kV, KBSI Gwangju Center). The electrical properties (i.e., carrier concentration, mobility, and resistivity) of the solution-based ATO thin films were measured using a Hall Effect Measurement System (Ecopia, HMS-3000). The optical properties in the wavelength range 300–900 nm were characterized using a UV-vis spectroscopy (Scinco, S-3100).

## 3. Results and discussion

Fig. 2 presents the XRD data obtained from samples A, B, C, and D. The bulk reflections for the reference pure  $\text{SnO}_2$  phases, which occur at 26.57°, 33.87°, and 51.75°, are shown at the bottom (JCPDS cards no. 21-1250). For all the samples, the main characteristic diffraction peaks at 26.69°, 33.90°, and 51.85° correspond to the (110), (101), and (211) planes of a tetragonal rutile structure of the cassiterite  $\text{SnO}_2$  phases (space

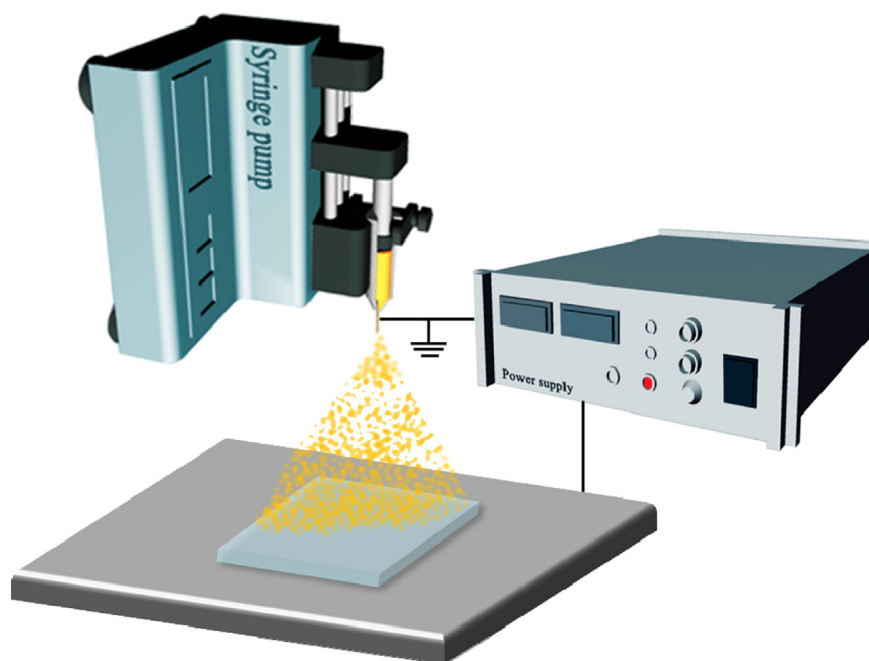


Fig. 1. Schematic illustration of an electro spray apparatus consisting of a power supply, a syringe with a pump, and a collector.

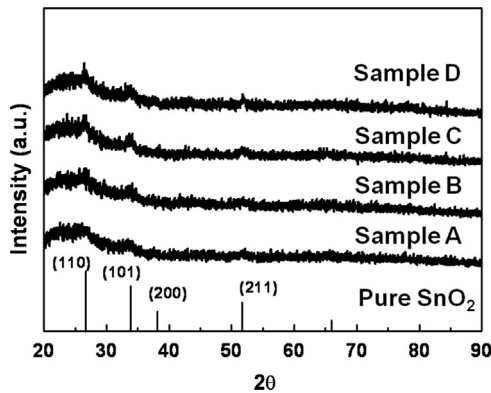


Fig. 2. XRD plots obtained from samples A, B, C, and D to investigate the structures and crystallinity. Reference bulk reflections of pure  $\text{SnO}_2$  phases are shown at the bottom (JCPDS cards no. 21-1250).

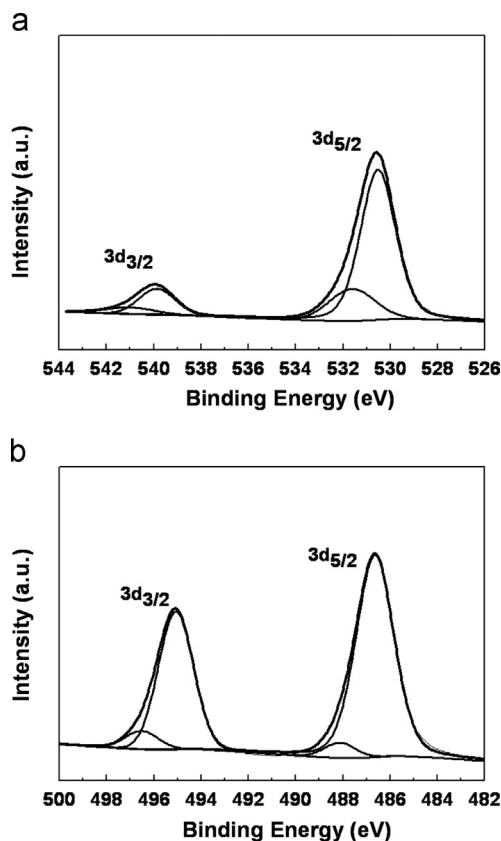


Fig. 3. XPS core-level spectra of the Sb  $3d$  (a) and Sn  $3d$  (b) photoelectrons obtained from sample C. (a) Sample C-Sb  $3d$  and (b) Sample C-Sn  $3d$ .

group  $P4_2/mnm$  [136]), which is slightly shifted to a higher angle compared to the pure  $\text{SnO}_2$  phases. This result implies that Sb ions are doped in the  $\text{SnO}_2$  lattice, which can be explained by Bragg's equation ( $n\lambda = 2d \sin \theta$ ); i.e., the diffraction peaks of the samples are shifted to the higher  $2\theta$  angle because the ionic radius of  $\text{Sb}^{5+}$  (0.62 Å) is smaller compared to that of  $\text{Sn}^{4+}$  (0.69 Å). In addition, all the samples exhibited low peak intensities because of the growth of thin (ca. 220–240 nm in thickness) and dense films.

XPS measurements were performed in order to examine the chemical composition and the chemical bonding states of sample C, obtained after calcination at 650 °C. Fig. 3(a) and (b) show the XPS core-level spectra of the Sb  $3d$  and Sn  $3d$  photoelectrons of the ATO thin films fabricated using electro spray. The Sb  $3d_{5/2}$  and Sb  $3d_{3/2}$  photoelectrons are emitted at  $\sim 530.5$  eV and  $\sim 539.3$  eV, implying Sb (V) in the  $\text{Sb}_2\text{O}_5$  phases. In addition, the Sn  $3d_{5/2}$  and Sn  $3d_{3/2}$  photoelectrons are at  $\sim 486.7$  eV and  $\sim 495.1$  eV, implying the existence of Sn (IV) species in the  $\text{SnO}_2$ . Thus, it is indicative that Sb ions in the ATO thin films exist as  $\text{Sb}^{5+}$ , which acts as donors in the  $\text{SnO}_2$  lattices. The samples are composed of  $\text{Sb}_2\text{O}_5$  and  $\text{SnO}_2$  phases, indicating the successful formation of Sb-doped  $\text{SnO}_2$  (ATO) thin films using electro spray.

Fig. 4(a)–(e) show the top-view FESEM images of the as-prepared sample before calcination, and samples A, B, C, and D. All samples fabricated using electro spray are uniformly formed on a glass substrate. With increasing calcination temperature, the grain sizes of the ATO nanoparticles increase gradually. Furthermore, the ATO thin films of sample D cracked because of high calcination temperature of 750 °C. ATO thin films that have cracks can lead to decreased Hall mobility, resulting in the reduction of electrical performance of the films. Fig. 4(f)–(j) show the cross-sectional FESEM images of the as-prepared sample before calcination, and samples A, B, C, and D. The thicknesses of the samples are in the range  $\sim 214$ – $228$  nm for the as-prepared sample before calcination,  $\sim 234$ – $240$  nm for sample A,  $\sim 212$ – $228$  nm for sample B,  $\sim 223$ – $235$  nm for sample C, and  $\sim 224$ – $234$  nm for sample D. The FESEM results confirmed that the samples with similar thickness exhibited uniform morphology. In particular, sample C exhibits high densification without formation of cracks. TEM measurements were performed to further investigate the grain sizes and crystallinity of ATO nanoparticles in the films.

Fig. 5(a)–(e) show the TEM images and SAED (selected area electron diffraction) patterns of samples A, B, C, and D. The particle sizes of the samples obtained using electro spray are in the range  $\sim 5.0$ – $6.5$  nm for sample A,  $\sim 6.9$ – $7.9$  nm for sample B,  $\sim 8.2$ – $16.4$  nm for sample C, and  $\sim 10.7$ – $14.0$  nm for sample D. It is indicative that as the calcination temperature increased, the sizes of the ATO nanoparticles also gradually increased. SAED patterns (the insets of Fig. 5), which are uniform ring patterns and diffraction spots, indicate that ATO nanoparticles are composed of a polycrystalline structure. Furthermore, as the size of ATO nanoparticles is increased, the diffraction patterns were gradually transformed from diffuse rings (sample A) to sharp rings containing clear spots (sample D). Thus, TEM and SAED results indicate the successful formation of polycrystalline ATO nanoparticles.

Fig. 6(a) presents the carrier concentration, the Hall mobility, and the resistivity of the samples. The carrier concentrations are observed to be  $\sim 1.45 \times 10^{20} \text{ cm}^{-3}$  for sample A,  $\sim 1.48 \times 10^{20} \text{ cm}^{-3}$  for sample B,  $\sim 1.83 \times 10^{20} \text{ cm}^{-3}$  for sample C, and  $\sim 4.23 \times 10^{20} \text{ cm}^{-3}$  for sample D. In addition, the mobilities of the samples are observed to be  $\sim 1.87 \text{ cm}^2/(\text{V s})$  for sample A,  $\sim 2.87 \text{ cm}^2/(\text{V s})$  for sample B,  $\sim 4.17 \text{ cm}^2/(\text{V s})$  for sample C, and  $\sim 1.04 \text{ cm}^2/(\text{V s})$  for

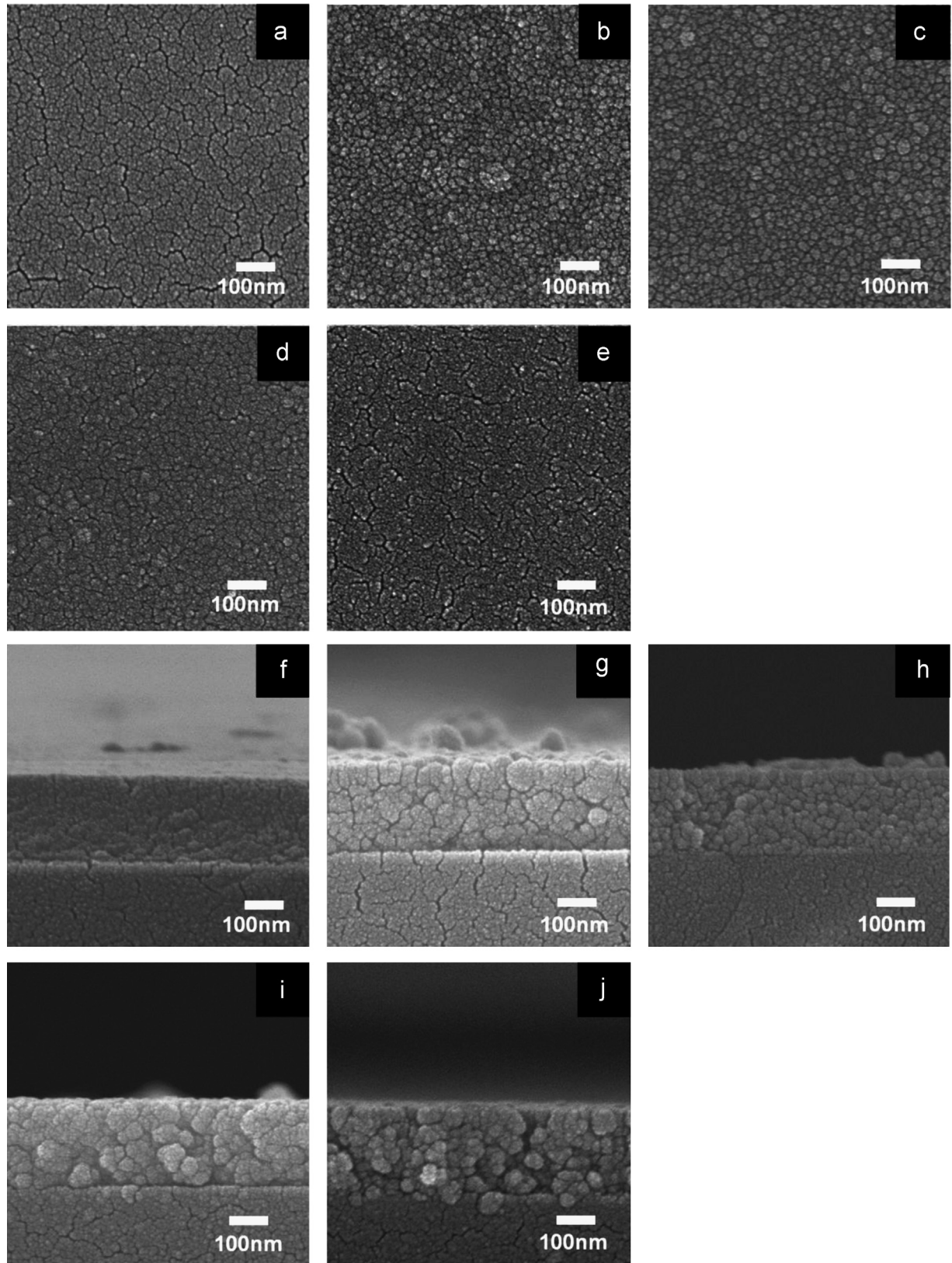


Fig. 4. Top-view FESEM images ((a)–(e)) and cross-section FESEM images ((f)–(j)) of as-prepared sample before calcination, and samples A, B, C, and D.

sample D. As the calcination temperature of the samples is increased, the carrier concentration and the mobility also gradually increased, which is directly related to the increased

diffusion of  $\text{Sb}^{5+}$  ions into the  $\text{SnO}_2$  matrix [15]. However, in spite of the highest calcination temperature, the mobility of sample D exhibits the lowest value because of the formation of

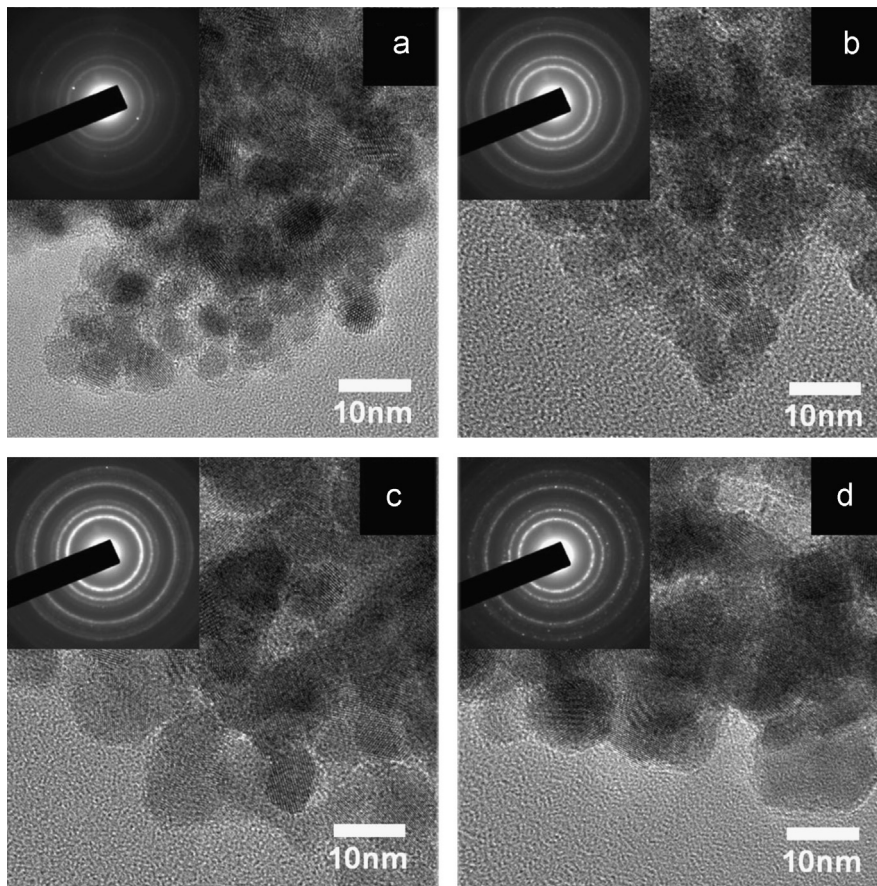


Fig. 5. TEM images ((a)–(d)) of ATO nanoparticles obtained from samples A, B, C, and D. SAED patterns of the samples are shown in the inset.

cracks along the grain boundaries on the ATO thin films, as shown in Fig. 4(e). That is, the cracks generated by gaps between the clusters of grains within the ATO thin films increased dramatically at a calcination temperature of 750 °C, which can cause the mobility drop. As a result, this phenomenon is directly related to the performance drop of the ATO thin films. The resistivity ( $\rho$ ) of the ATO thin films can be calculated using the following equation [3]:

$$\rho = 1/(Ne\mu)$$

where  $N$  is the carrier concentration,  $e$  is electron charge ( $1.602 \times 10^{-19}$  C), and  $\mu$  is the Hall mobility. Thus, the resistivities of the samples are  $\sim 2.33 \times 10^{-2} \Omega \text{ cm}$  for sample A,  $\sim 1.46 \times 10^{-2} \Omega \text{ cm}$  for sample B,  $\sim 8.14 \times 10^{-3} \Omega \text{ cm}$  for sample C, and  $\sim 1.04 \times 10^{-2} \Omega \text{ cm}$  for sample D. In other words, as the calcination temperature is increased, the resistivity of the samples is systematically decreased. However, sample D, which is calcined at 750 °C, shows an increased resistivity compared to sample C because it has the lowest mobility. It is noted that sample C exhibits the lowest resistivity compared to the other samples. The possible reason for improved resistivity is related to the high densification of the ATO thin films without formation of cracks, and the enhanced grain size of ATO nanoparticles. Fig. 6(b) shows the optical transmission spectra obtained from samples A, B, C, and D. All samples display excellent transmittance ( $\sim 90\%$  at

550 nm) because of the formation of dense thin films with almost similar film thicknesses. Most solution-based TCO thin films fabricated using methods, such as spray pyrolysis, sol-gel dip-coating, solvothermal, or ink-jet printing [11,16–18], showed low transmittances (i.e.,  $\sim 67\%$  to  $\sim 83\%$ ) compared to (i.e.,  $\sim 83\%$  to  $\sim 87\%$ ) the vacuum-based TCO thin films, such as chemical vapor deposition (CVD), sputtering, and pulsed laser deposition (PLD) [7,9–19]. However, the ATO thin films fabricated in this study using electrospray show a superior transmittance ( $\sim 90\%$  at 550 nm) despite being fabricated using a solution-based process. The electrical and optical results of all samples are summarized in Table 1. Fig. 6(c) presents the figure of merit (FOM) of samples A, B, C, and D that expresses the electrical and optical quality of the TCO thin films. FOM can be determined using the following equation [20]:

$$\text{FOM} = T^{10}/R_s$$

where  $T$  is the transmittance of the films and  $R_s$  is the sheet resistance. The higher the value of FOM, the better is the performance of the TCO thin films. The values of FOM are calculated as  $\sim 35.9 \times 10^{-5} \Omega^{-1}$  for sample A,  $\sim 54.9 \times 10^{-5} \Omega^{-1}$  for sample B,  $\sim 11.4 \times 10^{-4} \Omega^{-1}$  for sample C, and  $\sim 77.8 \times 10^{-5} \Omega^{-1}$  for sample D. Sample C exhibits the best FOM compared to the other samples, implying best performance of the TCO films. In particular, FOM fabricated

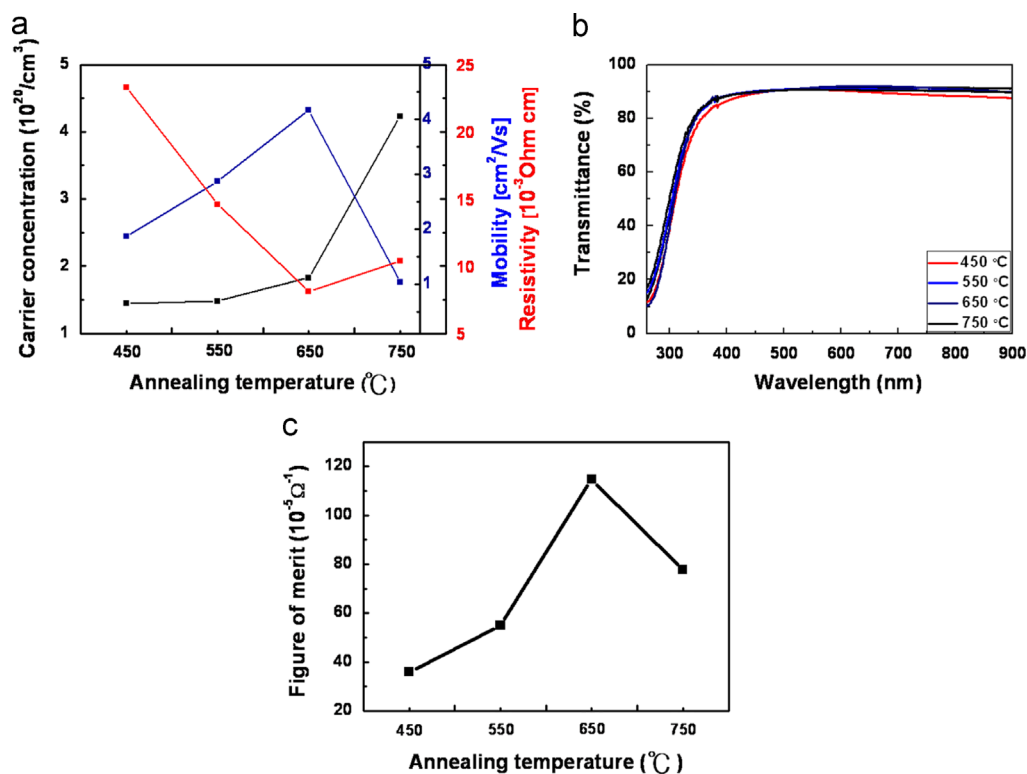


Fig. 6. Electrical properties for carrier concentration, the Hall mobility, and the resistivity (a), Optical transmission spectra (b), and figure of merit (c) of samples A, B, C, and D.

Table 1

Summary of electrical and optical properties for samples A, B, C, and D fabricated using electrospray.

Samples	Carrier concentration ( $\text{cm}^{-3}$ )	Hall mobility ( $\text{cm}^2/(\text{V s})$ )	Resistivity ( $\Omega\text{ cm}$ )	Transmittance (%)
Sample A	$1.45 \times 10^{20}$	1.87	$23.3 \times 10^{-3}$	90.7
Sample B	$1.48 \times 10^{20}$	2.87	$14.6 \times 10^{-3}$	90.9
Sample C	$1.83 \times 10^{20}$	4.17	$8.14 \times 10^{-3}$	91.4
Sample D	$4.23 \times 10^{20}$	1.04	$10.4 \times 10^{-3}$	90.6

by sputtering, spin coating, and ink-jet printing exhibited the values of  $\sim 10.0 \times 10^{-4} \Omega^{-1}$ ,  $\sim 11.0 \times 10^{-4} \Omega^{-1}$ , and  $\sim 0.6 \times 10^{-4} \Omega^{-1}$ , respectively. Thus, ATO thin films fabricated using electrospray showed excellent FOM compared to the other samples fabricated using above-mentioned techniques [21–23]. The results show that sample C exhibits superior resistivity ( $\sim 8.14 \times 10^{-3} \Omega\text{ cm}$ ), excellent transmittance ( $\sim 91.4\%$ ), and excellent FOM ( $\sim 11.4 \times 10^{-4} \Omega^{-1}$ ). Therefore, the electrospray technique is a promising tool for fabricating solution-based TCO thin films.

#### 4. Conclusions

Solution-based ATO thin films were fabricated using an electrospray method at four different calcination temperatures. Their structural, chemical, electrical, and optical properties were determined using XRD, XPS, FESEM, TEM, Hall effect measurement, and UV–vis spectroscopy. To elucidate the

optimum sample preparation conditions, four different calcination temperatures were used: 450 °C (sample A), 550 °C (sample B), 650 °C (sample C), and 750 °C (sample D). Sample C exhibits superior resistivity ( $\sim 8.14 \times 10^{-3} \Omega\text{ cm}$ ), transmittance ( $\sim 91.4\%$ ), and FOM ( $\sim 11.4 \times 10^{-4} \Omega^{-1}$ ) compared to the other samples because of the high densification and increased grain sizes of the ATO nanoparticles. Thus, solution-based ATO thin films fabricated using electrospray have the potential for use as TCOs in applications such as optoelectronics.

#### Acknowledgments

This work was supported by Grant no. 10041161 from the Ministry of Knowledge Economy (MKE) and Fundamental R&D Program for Core Technology of Materials funded by the Ministry of Knowledge Economy, Republic of Korea.

## References

- [1] S.H. Park, J.B. Park, P.K. Song, Characteristics of Al-doped, Ga-doped and In-doped zinc-oxide films as transparent conducting electrodes in organic light-emitting diodes, *Current Applied Physics* 10 (2010) S488–S490.
- [2] D. Slocombe, A. Porch, M. Pepper, P.P. Edwards, The Mott transition and optimal performance of transparent conducting oxides in thin-film solar cells, *Energy and Environmental Science* 5 (2012) 5387–5391.
- [3] S. Calnan, A.N. Tiwari, High mobility transparent conducting oxides for thin film solar cells, *Thin Solid Films* 518 (2010) 1839–1849.
- [4] C. Guillen, J. Herrero, TCO/metal/TCO structures for energy and flexible electronics, *Thin Solid Films* 520 (2011) 1–17.
- [5] T.R. Giraldi, M.T. Escote, M.I.B. Bernardi, V. Bouquet, E.R. Leite, E. Longo, J.A. Varela, Effect of thickness on the electrical and optical properties of Sb doped SnO<sub>2</sub> (ATO) thin films, *Journal of Electroceramics* 13 (2004) 159–165.
- [6] K. Ravichandran, P. Philominathan, Fabrication of antimony doped tin oxide (ATO) films by an inexpensive, simplified spray technique using perfume atomizer, *Materials Letters* 62 (2008) 2980–2983.
- [7] J. Kane, H.P. Schweizer, W. Kern, Chemical vapor deposition of antimony-doped tin oxide films formed from dibutyl tin diacetate, *Journal of The Electrochemical Society* 123 (1976) 270–277.
- [8] E.K. Shokr, Optimization of the electrical and optical properties of Sb–Sn–O thin films, *Semiconductor Science and Technology* 15 (2000) 247–253.
- [9] S.U. Lee, W.S. Choi, B. Hong, Synthesis and characterization of SnO<sub>2</sub>:Sb film by dc magnetron sputtering method for applications to transparent electrodes, *Physica Scripta T129* (2007) 312–315.
- [10] D. Burgard, C. Goebbert, R. Nass, Synthesis of nanocrystalline, redispersible antimony-doped SnO<sub>2</sub> particles for the preparation of conductive, transparent coatings, *Journal of Sol–Gel Science and Technology* 13 (1998) 789–792.
- [11] H. Bisht, H.T. Eun, A. Mehrtens, M.A. Aegerter, Comparison of spray pyrolyzed FTO, ATO and ITO coatings for flat and bent glass substrates, *Thin Solid Films* 351 (1999) 109–114.
- [12] L. Dua, P.K. Biswas, Synthesis and characterization of nanostructured Mn(II) doped antimony-tin oxide (ATO) films on glass, *Applied Surface Science* 280 (2013) 33–41.
- [13] D. Zhang, L. Tao, Z.B. Deng, J.B. Zhang, L.Y. Chen, Surface morphologies and properties of pure and antimony-doped tin oxide films derived by sol-gel dip-coating processing, *Materials Chemistry and Physics* 100 (2006) 275–280.
- [14] S.J. Jeon, J.J. Lee, J.T. Kim, S.M. Koo, Stable antimony-doped tin oxide nano-sols and their films produced by a sol-coating method, *Journal of Ceramic Processing Research* 7 (2006) 321–326.
- [15] J.W. Leem, J.S. Yu, Physical properties of electrically conductive Sb-doped SnO<sub>2</sub> transparent electrodes by thermal annealing dependent structural changes for photovoltaic applications, *Materials Science and Engineering B* 176 (2011) 1207–1212.
- [16] C. Terrier, J.P. Chatelon, R. Berjoan, J.A. Roger, Sb-doped SnO<sub>2</sub> transparent conducting oxide from the sol–gel dip coating technique, *Thin Solid Films* 263 (1995) 37–41.
- [17] L. Lili, M. Liming, D. Xuechen, Solvothermal synthesis and characterization of Sb-doped SnO<sub>2</sub> nanoparticles used as transparent conductive films, *Materials Research Bulletin* 41 (2006) 541–546.
- [18] J.W. Lim, B.Y. Jeong, H.G. Yoon, S.N. Lee, J.H. Kim, Inkjet-printing of antimony-doped tin oxide (ATO) films for transparent conducting electrodes, *Journal of Nanoscience and Nanotechnology* 12 (2012) 1675–1678.
- [19] F. Chen, N. Li, Q. Shen, C. Wang, L. Zhang, Fabrication of transparent conducting ATO films using the ATO sintered targets by pulsed laser deposition, *Solar Energy Materials and Solar Cells* 105 (2012) 153–158.
- [20] J. Liu, A.W. Hains, J.D. Servaites, M.A. Ratner, T.J. Marks, Highly conductive bilayer transparent conductive oxide thin films for large-area organic photovoltaic cells, *Chemistry of Materials* 21 (2009) 5258–5263.
- [21] S.U. Lee, W.S. Choi, B.Y. Hong, Synthesis and characterization of SnO<sub>2</sub>:Sb film by dc magnetron sputtering method for applications to transparent electrodes, *Physica Scripta T129* (2007) 312–315.
- [22] T.R. Giraldi, M.T. Escote, M.I.B. Bernardi, V. Bouquet, E.R. Leite, E. Longo, J.A. Varela, Effect of thickness on the electrical and optical properties of Sb doped SnO<sub>2</sub> (ATO) thin films, *Journal of Electroceramics* 13 (2004) 159–165.
- [23] J.W. Lim, B.Y. Jeong, H.G. Yoon, S.N. Lee, J.H. Kim, Inkjet-printing of antimony-doped tin oxide (ATO) films for transparent conducting electrodes, *Journal of Nanoscience and Nanotechnology* 12 (2012) 1675–1678.